Variability in aerosol optical properties and radiative forcing over Gorongosa (18.970S, 34.350E) in Mozambique

Article *in* Meteorology and Atmospheric Physics · April 2015

DOI: 10.1007/s00703-014-0352-2

CITATIONS
5

READS
81

3 authors:

Joseph Adesina
North West University South Africa
16 PUBLICATIONS **64** CITATIONS
SEE PROFILE

Raghavendra KUMAR Kanike
Nanjing University of Information Science & …
38 PUBLICATIONS **565** CITATIONS
SEE PROFILE

Venkataraman Sivakumar
University of KwaZulu-Natal
116 PUBLICATIONS **521** CITATIONS
SEE PROFILE

Variability in aerosol optical properties and radiative forcing over Gorongosa (18.97°S, 34.35°E) in Mozambique

A. Joseph Adesina, K. Raghavendra Kumar & V. Sivakumar

Meteorology and Atmospheric Physics

ISSN 0177-7971
Volume 127
Number 2

Meteorol Atmos Phys (2015)
127:217-228
DOI 10.1007/s00703-014-0352-2

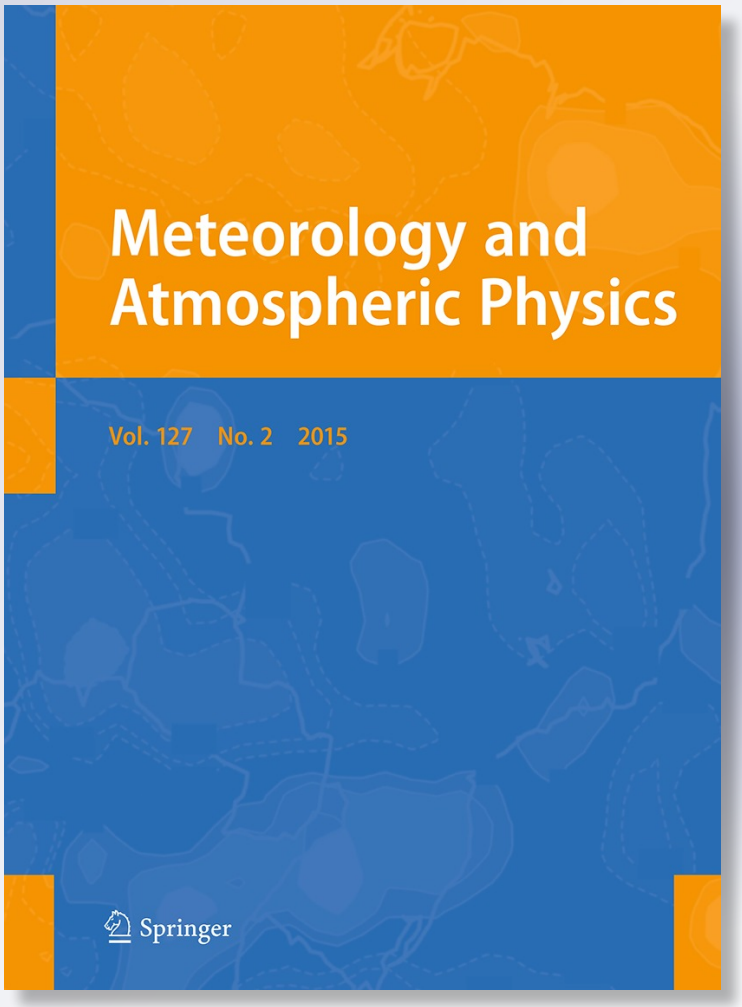

Springer

Meteorol Atmos Phys (2015) 127:217–228
DOI 10.1007/s00703-014-0352-2

ORIGINAL PAPER

Variability in aerosol optical properties and radiative forcing over Gorongosa (18.97°S, 34.35°E) in Mozambique

A. Joseph Adesina · K. Raghavendra Kumar · V. Sivakumar

Received: 6 April 2014 / Accepted: 15 October 2014 / Published online: 25 October 2014

Abstract This paper reports the observational results of aerosol optical, microphysical and radiative characteristics for the time measured over Gorongosa (18.97°S, 34.35°E, 30 m asl) in Mozambique using a ground-based AERONET sun-sky radiometer. In the present study, the data recorded during the period July–December, 2012 have been used and particular attention was paid to show how aerosol loading evolves during the biomass burning season (spring) including pre- and post-months. The results reveal that the monthly mean aerosol optical depth (AOD) at 500 nm was high (low) with 0.64 ± 0.34 (0.20 ± 0.06) in September (November), while the Ångström Exponent (AE) ($\alpha_{440-870}$) decreased, except September (1.56 ± 0.26) due to increase in the fine-mode aerosol concentration produced from biomass burning. The volume size distribution (VSD) has bimodal lognormal structure and has fine-mode (coarse) maximum at a radius of 0.15 μm (3.0 μm) in September (December). The single scattering albedo (SSA) decreases with wavelength from July to October and almost stable in November and December. The imaginary (Im) refractive index (RI) showed a strong evidence of black carbon aerosol origin during the biomass burning months. Aerosol radiative forcing (ARF) computed from SBDART model shows large negative values at the surface (−89.22 W m^{-2}) and at the top (−22.36 W m^{-2}), with a higher value of atmospheric forcing (+66.87 W m^{-2}) resulting in average tropospheric heating rate of 1.88 K day^{-1} for the study period. Further, the comparison shows good agreement between the ARFs at the top and bottom of the atmosphere derived from AERONET to SBDART.

Responsible Editor: S. T. Castelli.

A. J. Adesina · V. Sivakumar
Discipline of Physics, School of Chemistry and Physics, College of Agriculture, Engineering and Science, Westville Campus, University of KwaZulu–Natal, Durban 4000, South Africa

K. R. Kumar (✉)
Key Laboratory for Aerosol-Cloud-Precipitation of China Meteorological Administration, School of Atmospheric Physics, Nanjing University of Information Science and Technology, Nanjing 210044, Jiangsu, China
e-mail: kanike.kumar@gmail.com; krkumar@nuist.edu.cn

1 Introduction

Atmospheric aerosols play an important role in the Earth's radiation budget by exerting direct and indirect radiative forcing of climate (Charlson et al. 1992; Satheesh and Moorthy 2005; Jayaraman et al. 2006; Alam et al. 2012; Sinha et al. 2013), contributing to significant heating in the troposphere (Babu et al. 2011; Alam et al. 2011) as well as affecting the hydrological cycle and precipitation rates (Rosenfeld et al. 2001; Ramanathan et al. 2001). Aerosols, which are fine particles suspended in the air, comprise of mixture of mainly sulphates, nitrates, sea salt, mineral dust and carbonaceous (organic and black carbon) particles. Black carbon (BC) is a bi-product from incomplete combustion of coal, diesel engines, biofuels and outdoor biomass burning. Biomass burning is produced from increase use of firewood for domestic fuel and clearing of forest lands for agriculture by slash and burning to meet the demands of expanding population. It produces large amounts of trace gases and aerosol particles (BC), which play a pivotal role in tropospheric chemistry and climate (Arola et al. 2007).

BC particles produced from biomass burning are of special interest as they absorb sunlight, heat the air and contribute to global warming, unlike most aerosols which reflect sunlight to space and have cooling effect (Arola et al. 2011;

Bond et al. 2013 and references therein). The main source areas of emissions of BC particles are the tropical and subtropical regions (25°S–25°N) where forest fires are associated with local and regional farming activities. More than 80 % of this burning is in the tropical regions and these submicron smoke particles may have a significant impact on climate by altering the global radiation balance (Badarinath et al. 2009; Kumar et al. 2010; Gadhavi and Jayaraman 2010). The direct radiative effect of smoke from biomass burning and the indirect effect through clouds may be of equal significance to climate (Penner et al. 1992). A high optical depth of aerosol due to biomass burning has epidemiological (as in respiratory diseases), physical (as in visibility) and climatic effects (Eck et al. 2003a; Roberts et al. 2011).

In Southern Africa, the farming activities go on mainly in the dry season with few fires in the wet season (Archibald et al. 2012). Studies show that Southern Africa savannah smoke is the most absorbing of all other major biomass burning regions (Dubovik et al. 2002). To date, there have been several studies on aerosols in southern part of Africa [Eck et al. 2003a, b, 2013; Ogunjobi et al. 2008; Sivakumar et al. 2010; Queface et al. 2011; Tesfaye et al. 2011; Kumar et al. 2013; Adesina et al. 2014 (In Press)]. To the best of our knowledge, no study yet has been conducted to characterise aerosol optical properties and estimation of aerosol radiative forcing (ARF) over Gorongosa. The present study will enable a better understanding of both the regional and local behaviour of aerosol over Mozambique region.

In this study, we used Aerosol Robotic Network (AERONET) data (Holben et al. 1998) of version 2.0 level 1.5 and the results are reported for the first time over Gorongosa in Mozambique by analysing the aerosol optical properties with the aim to investigate the monthly variations in aerosol optical depth (AOD), Ångström exponent (AE) and columnar water vapour (CWV). We also analyse the seasonal variability of volume size distribution (VSD) of aerosols, and investigate the variability of single scattering albedo (SSA), asymmetry parameter (g) as well as real (Re) and imaginary (Im) parts of the refractive index (RI). The aerosol radiative forcing (ARF) computations have been carried out using the Santa Barbara DISORT Atmospheric Radiative Transfer (SBDART) model (Ricchiazzi et al. 1998). Finally, the ARFs of AERONET and SBDART have been compared at the top and bottom of atmosphere.

2 AERONET site and instrumentation

2.1 Site description

Mozambique, lying between latitudes 10°S and 27°S and longitudes 30°E and 41°E, is a country located on the Southeast coast of Africa (see Fig. 1). It is located in the Inter-Tropical Convergence Zone (ITCZ), having a tropical climate, which makes the exact onset of seasons depend on the particular location in the country. It has two major seasons, wet season from November to March with high relative humidity and frequent rains and the dry season from April to October. The study region has been affected with strong and severe seasonal biomass burning and/or forest fires every year during dry period (September and October).

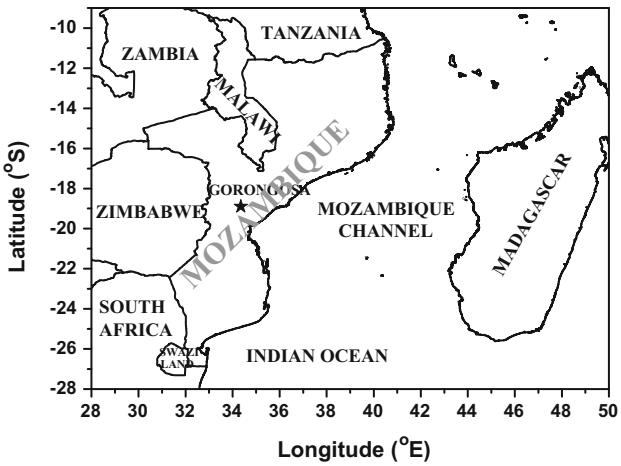

Fig. 1 Location map of the AERONET site in Mozambique along with the surrounding waters and bordering countries. The *star* denotes the geographical position of the study region (Gorongosa)

Gorongosa (18.97°S, 34.35°E, 30 m asl) is located at the southern end of the Great African Rift Valley in the heart of central Mozambique (see Fig. 1) with a National Park nestled in a 4,000 km^2 section of it and a river originates from Mount Gorongosa. It is humid with an average level of rainfall ranging between 900 mm and 1,000 mm. The average temperature in the month of June is about 28 °C and decreases to about 26 °C in July and August with a little chance of rain (figure not shown). Rain is being expected at the end of September as temperature goes to about 30 °C and by October showers are already approaching. November and December are summer months which have both rain and sun and the temperature may go up to about 32 °C on the average.

2.2 AERONET sun-sky radiometer

The observations are carried out with an AERONET sun-sky radiometer of CIMEL (CE–318) make installed on the roof top of workshop area, approximately 6 m high which is located at Chitengo camp, Gorongosa National Park surrounded with few trees in immediate vicinity. Frequent grass fires in the park from August to November and burning of waste periodically approximately 300 m away

surrounds the measurement site. AERONET is a global network of sun-sky radiometers (Holben et al. 1998). The calibrated and quality-checked data are available online at http://aeronet.gsfc.nasa.gov/. The AERONET sun-sky radiometer is being used to take measurements of both direct sun and diffuse sky radiances. The sun measurements are taken at nine wavelengths, in which eight specific wavelengths (340, 380, 440, 500, 675, 870, 940 and 1,020 nm) are used to estimate aerosol optical properties, with 940 nm bandwidth designed to retrieve CWV (Kumar et al. 2013). The sky radiance measurements are obtained at four wavelengths (440, 675, 870, and 1,020 nm) through a large range of scattering angles from the Sun (Dubovik et al. 2000, 2002). A number of studies have already described the sun-sky radiometer, data acquisition, and retrieval algorithms, calibration procedures, which confirm to the standards of the AERONET, as well as the uncertainty in final products and applied cloud-screening procedures (Holben et al. 1998, 2006; Eck et al. 1999; Dubovik and King 2000; Dubovik et al. 2002; Sumit Kumar et al. 2011; Alam et al. 2012; Kumar et al. 2013 and references within); however, a brief description is presented here.

The uncertainty in retrieval under cloud-free conditions for AOD is less than ±0.01 for the wavelengths greater than 0.44 μm and generally less than ±0.02 for shorter wavelengths, while that of sky radiance measurements are less than ±0.05 (Eck et al. 1999; Dubovik et al. 2000). The version 2.0 used in the AERONET data retrieval utilises a bidirectional reflectance distribution function (BRDF) that allows for dynamic reflectance as a function of zenith angle of the sun over land and water. AOD is obtained from the direct sun measurements while SSA, refractive indices (real and imaginary) and VSD are obtained from the inversion products. Level 1.5 AERONET data (cloud screened but not quality checked, Smirnov et al. 2002 from July to December, 2012 have been used in this study, as level 2.0 data are not available or released in the AERONET website over this site from both direct sun and inversion products. We used AOD at five wavelengths (440, 500, 675, 870 and 1,020 nm) along with AE (440–870), SSA, g and complex RI at four wavelengths (440, 675, 870 and 1,020 nm). We have also used true colour composite fire images derived from the MODIS Aqua satellite obtained for the month of September during the last one decade (2002–2013) to show evidence of increased biomass burning and forest fires over Mozambique and in Southern Africa during dry months.

2.3 NCEP/NCAR reanalysis winds

The surface wind flow patterns obtained from NCEP/NCAR (National Center for Environmental Prediction/National Center for Atmospheric Research) reanalysis with a spatial resolution of 2.5° × 2.5° at a pressure level of 850 hPa are also used to ascertain the synoptic meteorological conditions and source variability during the study period (Kalnay et al. 1996). The data have been downloaded from the website www.cdc.noaa.gov.

Table 1 Monthly mean of AOD, CWV and $\alpha_{440-870}$ along with the standard deviations from the mean

Month	AOD_{500}	CWV (cm)	$\alpha_{440-870}$
July	0.24 ± 0.12	1.88 ± 0.28	1.54 ± 0.24
August	0.40 ± 0.26	2.18 ± 0.44	1.52 ± 0.26
September	0.64 ± 0.34	2.68 ± 0.34	1.56 ± 0.26
October	0.38 ± 0.16	2.71 ± 0.59	1.48 ± 0.44
November	0.20 ± 0.06	3.06 ± 0.57	1.22 ± 0.16
December	0.24 ± 0.24	4.02 ± 0.77	0.76 ± 0.34

2.4 HYSPLIT trajectories

The Hybrid Single Particle Lagrangian Integrated Trajectory (HYSPLIT) model is the latest version of an integrated system for computing air parcel trajectories, dispersion and deposition simulations (Draxler and Rolph 2003). The 7-day time period (168 h) is applied to derive the air mass back trajectories (http://http://ready.arl.noaa.gov/HYSPLIT.php), since the typical residence time for aerosols in the lower troposphere is 5–7 days.

3 Results and discussion

3.1 Variability in aerosol optical properties and columnar water vapour

Aerosol optical properties are characterised by AOD and Angstrom exponent (AE, α), derived from a multispectral log–log linear fit to τ_a–$\lambda^{-\alpha}$ based on four wavelength range (440–870 nm) (Ångström 1961; Shaw 1983; Gupta et al. 2003; Bi et al. 2011). Table 1 shows the monthly variation of AOD at 500 nm, AE ($\alpha_{440-870}$) and CWV for the study period and the value next to ± sign represents the standard deviation of the mean. AOD which is strongly dependent on wavelength can be used to identify both the evolution and source region of aerosol as it represent the airborne particles loading in the atmospheric column (Kumar et al. 2013 and references therein). This implies that for shorter wavelengths AOD values are higher than at longer wavelengths (Kumar et al. 2013; Alam et al. 2011). Furthermore, the spectral dependence of AOD is a function of aerosol particle-size distribution (Suman et al. 2013).

It is clearly evident from Table 1 that the monthly mean values of AOD_{500} vary considerably with the highest of 0.64 ± 0.34 observed in September and the lowest of 0.20 ± 0.06 in November. The result is comparable to that of the regions Mongu and Skukuza (Queface et al. 2011; Kumar et al. 2013; Eck et al. 2013) in South Africa with identical regional climate. The AOD recorded a sharp increase from July to a maximum in September, and then decreases in October attaining a minimum value in November with a small increase in AOD again during December. The local and regional pollutants along with atmospheric convection might play a major role in the increase in AOD during December. The factors responsible for seasonal variation are the frequent biomass burning and forest fire activities during the dry period.

Fire detection and monitoring by satellite remote sensing use information of thermal sensor radiance data. To show evidence for the high aerosol loading during spring (September and October months), the fire images showing the red hot spots are obtained from NASA's EOS MODIS rapid response which delivers global hotspots or fire locations through Terra/Aqua satellites at local overpass time (https://earthdata.nasa.gov/data/near-real-time-data/rapid-response). Figure 2 shows the true colour composite maps (band 1-4-3) of active fire locations as detected by Aqua-MODIS over Mozambique at 2 km resolution at local overpass time. The first panel in the top row denotes the fire hot spot locations over Mozambique and surrounding regions in the southern part of Africa as identified by MODIS Aqua satellite for the entire month of September in 2012. Similarly, the fire locations monitored by MODIS Aqua satellite for a typical day in the month of September during 2002–2013 are also shown in Fig. 2 (a–k), except for the year 2005, as no image has been derived from MODIS Aqua sensor. It is clearly depicted from all the figures that there are large number of fire hot spots during September every year resulting from forest fires and/or biomass burning activities over Mozambique and other parts of Africa resulted an increase in the aerosol loading. In addition to this, fresh smoke particles emitted from the fires observed over Madagascar (see Fig. 2) are also transported towards the measurement site during the biomass burning period under favourable winds. Thus, the observations showing high AOD in the September month which is fairly significant with the MODIS fire maps derived from the Aqua satellite.

To understand the role of surface winds stated in the above section, synoptic wind patterns have been obtained from NCEP/NCAR reanalysis data to represent the magnitude and direction of winds for each month during the study period. The contour and length of the arrow represents the magnitude of wind speed in m s^{-1} and the direction of the arrow indicates the wind direction over the region. It is depicted from the figure that high winds in the month of September (Fig. 3c) and October (Fig. 3d) directed from easterlies transport fresh smoke particles generated at Madagascar towards the measurement site. Thus, meteorology also favours for the observed high AOD during the dry period over the study region. Furthermore, the HYSPLIT air mass back trajectories downloaded from NOAA ARL website also support for the measured high and low AODs during the study period. The back trajectories computed at three different heights 500 m, 1,500 m and 3,000 m asl for a typical day in each month from July to December, 2012 also show the possible transport of air parcels from the source region to the study location (Fig. 4a–f). During the dry months (September and October), the air mass trajectories at all levels are originated from Madagascar and the mainland of Africa taking fresh smoke particles generated from forest fires and/or biomass burning activities towards the experimental region, which results in high AOD; whereas in November and December, the air mass pathways are coming from the oceanic environment (Indian Ocean) having long trajectory history bringing coarse-mode sea-salt particles. These particles having smaller residence times settle down before reaching the measurement site resulting in low AOD.

Ångström exponent (AE, $\alpha_{440-870}$) is a function of aerosol particle size (Gadhavi and Jayaraman 2010). High values of AE indicate the dominance of fine particles, whereas low values indicate the dominance of coarse particles and relatively lower concentration of fine particles. AE was found to be high (>1.4) from July to October (Table 1) which shows the presence of fine particles and from November (1.22) it started to decrease with a low value in December (0.78) which indicates a shift to the coarse mode as the fine particles might have been removed by deposition (Suman et al. 2013). The CWV associated with the seasonality in precipitation constantly increased from July to December with the lowest value of 1.88 ± 0.28 cm in July and the highest of 4.02 ± 0.77 cm in December (see Table 1). This difference in CWV was also reported by Jayaraman et al. (1998) over polar and subtropical/tropical regions. One would expect aerosol particle to become larger due to hygroscopic growth in the presence of higher amount of water vapour (Ranjan et al. 2007), but persistence of fine particles until December implies that water vapour and aerosol may be located at different heights and are not well mixed. Also, non-hygroscopic particle will not grow in the presence of water vapour which is the case with most of BC particles.

3.2 Volume size distribution (VSD)

The size distribution of aerosols is an important parameter in understanding their effect on the climate. Figure 5 shows

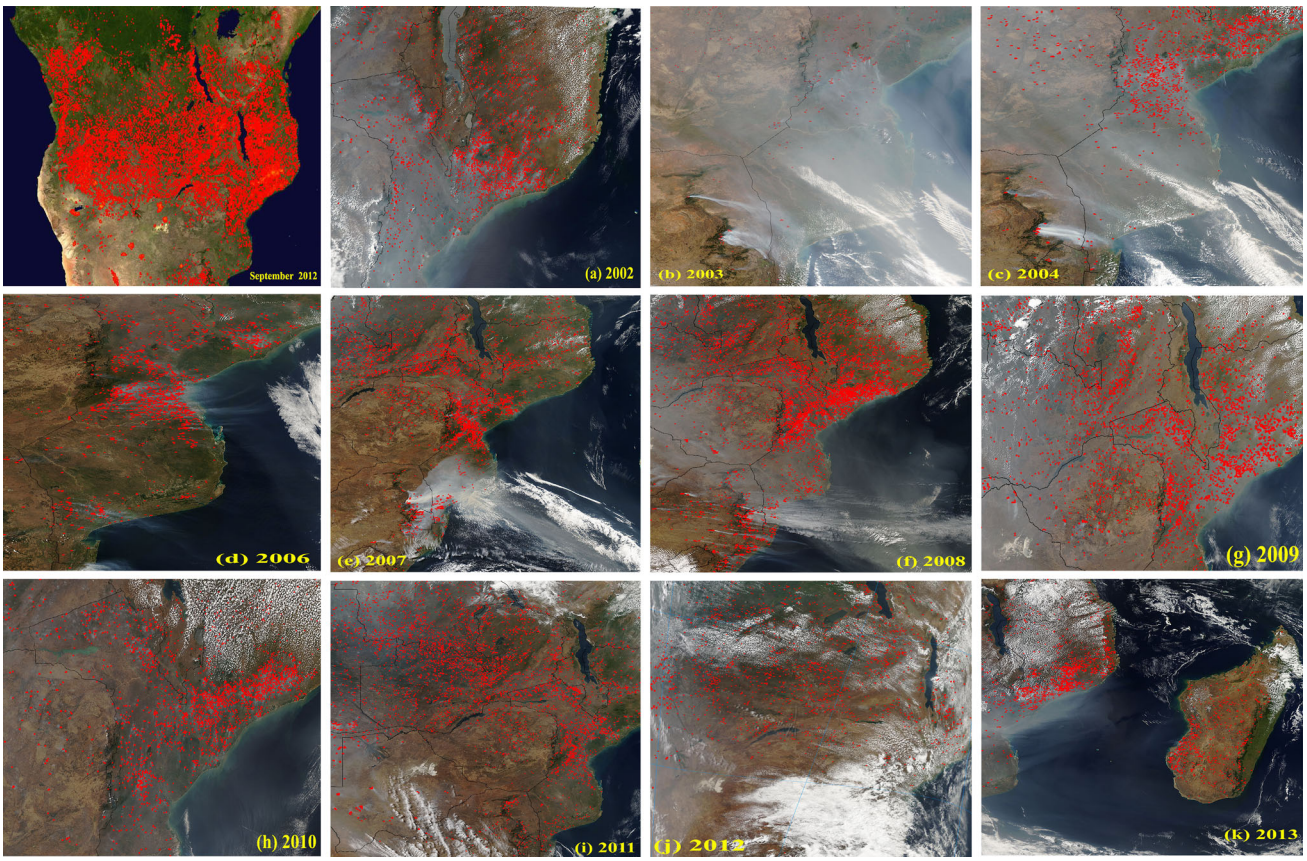

Fig. 2 True colour composite images of fire hotspots derived from Aqua-MODIS over Mozambique and its surrounding regions for the entire month of September, 2012 (First panel on the *top row*). Fresh smoke and fire hot spots detected from MODIS onboard Aqua satellite at local overpass time with 2 km resolution over Mozambique and surroundings for a typical day in the month of September during 2002–2013 (**a**–**k**)

the monthly average volume size distribution (dV/dlnR) of aerosols with vertical bars representing the standard deviation of the mean. The variations in these distributions are largely associated with changes in the amplitude and spectral dependence of the AOD. The fine mode ($r < 0.6$ μm) changes significantly, while the coarse mode ($r > 0.6$ μm) shows relative stability. The fine mode with a radius of about 0.15 μm (0.1 μm) has its highest (lowest) values in September (December), while the coarse mode with a radius of about 3.5 μm (4 μm) has its highest (lowest) values in December (July). The bimodal structure of the VSD shows that the aerosol has a mixture of coarse particles which are of sea salt or mineral dust in all the months. Similar observations have been reported by Dubovik et al. (2002) over worldwide locations.

3.3 Single scattering albedo and asymmetry parameter

The aerosol single scattering albedo (SSA), defined as the ratio between the particle scattering coefficient and total extinction coefficient, is usually used to characterise the aerosol absorption properties and is a key variable in assessing the ARF. When dust is not a major contributor to the atmospheric aerosol, the SSA decreases with wavelength (D'Almeida et al. 1991; Hess et al. 1998). In Fig. 6a, two major features of SSA spectral dependence can be observed. The SSA decreases with wavelength from July to September with intermittent values in the October month, while for November and December the spectral dependence is almost neutral except for a slight increase for the wavelengths beyond 875 nm. The above results are comparable to the work carried out by Eck et al. (2003b) at Inhaca Island, Mozambique.

The asymmetry parameter (g) is defined as the intensity-weighted average cosine of the scattering angle:

$$g = \frac{1}{2}\int_0^{\pi} \cos\theta P(\theta)\sin\theta d\theta \quad (1)$$

where θ is the angle between the incident light and scattering direction and $P(\theta)$ is the angular distribution of scattered light (the phase function). The value of g ranges

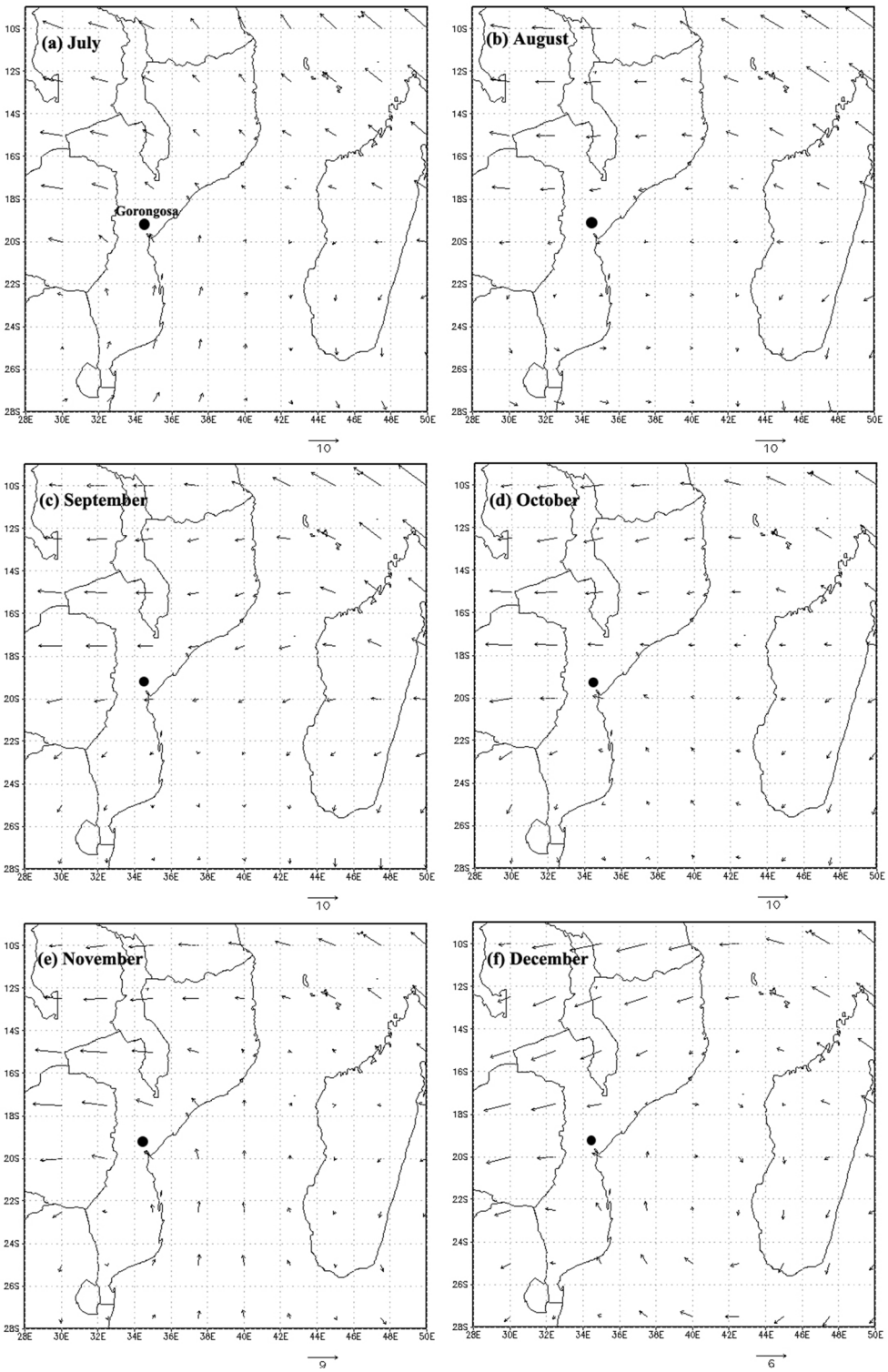

Fig. 3 NCEP/NCAR synoptic wind patterns for different months during July–December, 2012. The *black solid circles* in all the panels represent the geographical location of the study region

between −1 for entirely backscattered light to +1 for entirely forward scattered light. At 500-nm wavelength, it ranges between 0.64 and 0.83 at low relative humidity and between 0.64 and 0.82 at high relative humidity. It is a key parameter in radiative forcing and depends on both the size distribution and composition of aerosols (Andrews et al. 2006; Ramachandran and Rajesh 2008).

The asymmetry parameter (g) is spectral dependent (decrease with increasing wavelengths) as shown in Fig. 6b. The negative gradient is more pronounced in

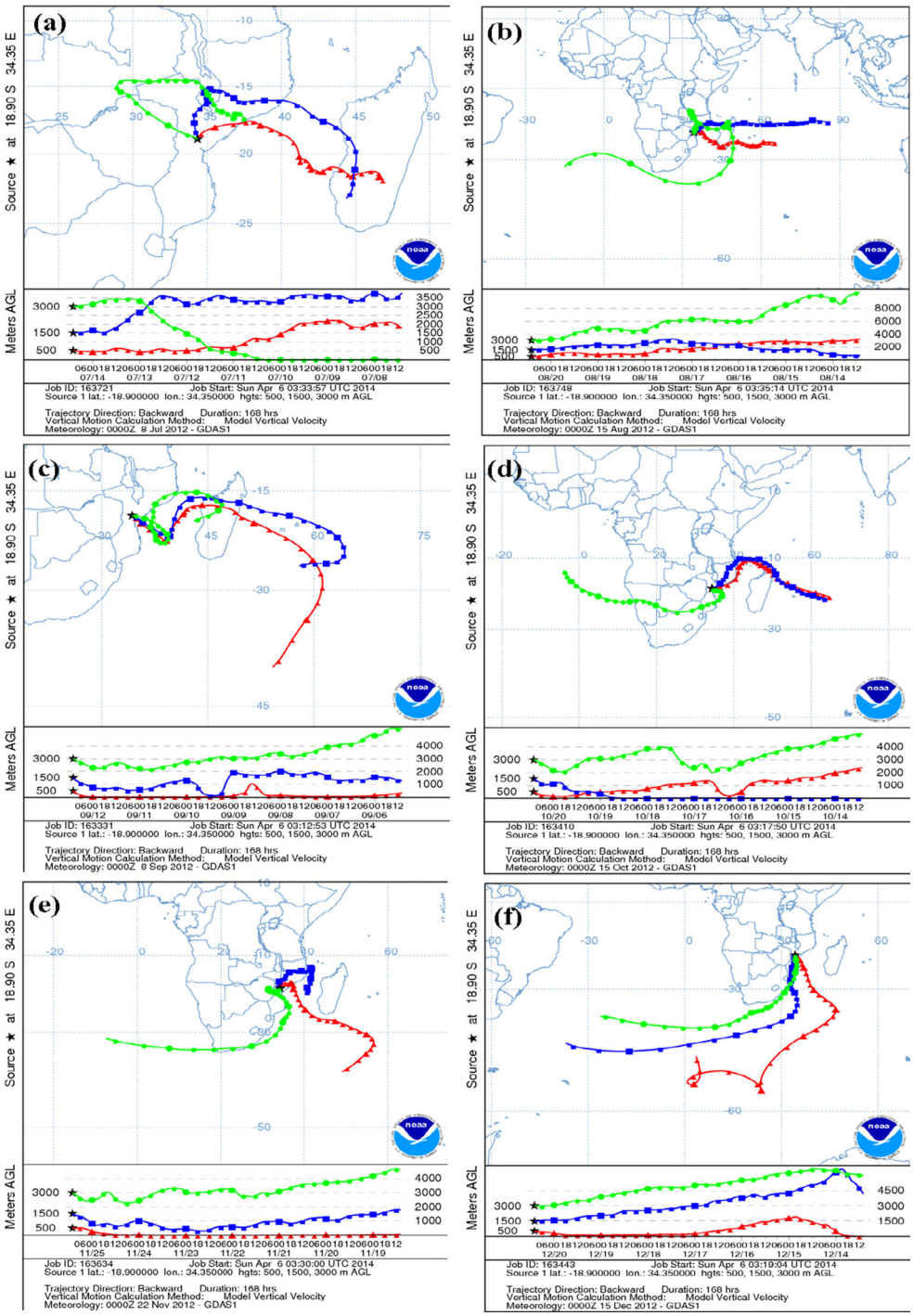

Fig. 4 HYSPLIT back trajectories representing the air mass pathways at three different heights over Gorongosa on a typical day in each month during the study period July–December, 2012 (**a**–**f** in sequence)

September where the value decreased from 0.68 ± 0.02 at 440 nm to 0.56 ± 0.06 at 1,020 nm, while in December it increased from 0.72 ± 0.03 at 440 nm to 0.73 ± 0.03 at 1,020 nm. This decrease can be seen in July and August, while it is not so pronounced in October. The decrement suggests that during July and August months anthropogenic absorbing aerosol are relative in abundance, while the increase in the near-IR region in November and December suggests the relative abundance of coarse-size particle (Alam et al. 2012; Srivastava et al. 2011).

3.4 Refractive indices

The real (Re) and imaginary (Im) parts of complex refractive indices reflect the ability of scattering and absorption to incoming radiation, respectively. The

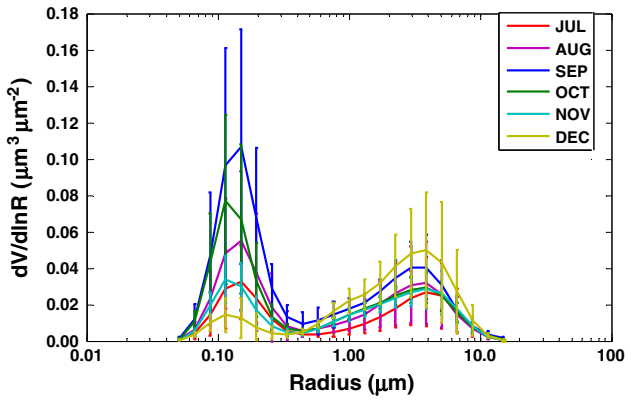

Fig. 5 Monthly variations in aerosol volume size distribution. The *vertical bars* indicate ±1σ standard deviation from the mean

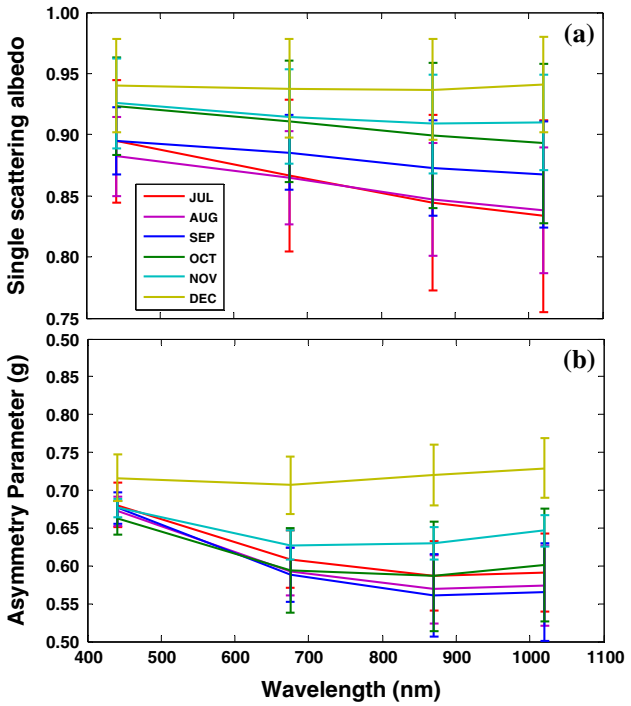

Fig. 6 Spectral variations of single scattering albedo (**a**) and asymmetry parameter (**b**) at four wavelengths during the study period

monthly average values of the real part vary within 1.43–1.48 at shorter wavelengths (440 nm) and 1.43–1.49 at longer wavelengths (1,020 nm) which is clearly shown in Fig. 7a. The average values of the imaginary part are relatively large from July to September ranging from 0.015 to 0.019 at 440 nm (Fig. 7b). This suggests that the aerosols present are absorbing type and the values range between 0.003 and 0.008 for October to December indicating coarse dust particle of reflecting type (Bi et al. 2011; Suman et al. 2013). The results support that aerosol type is of BC originated from biomass burning during September

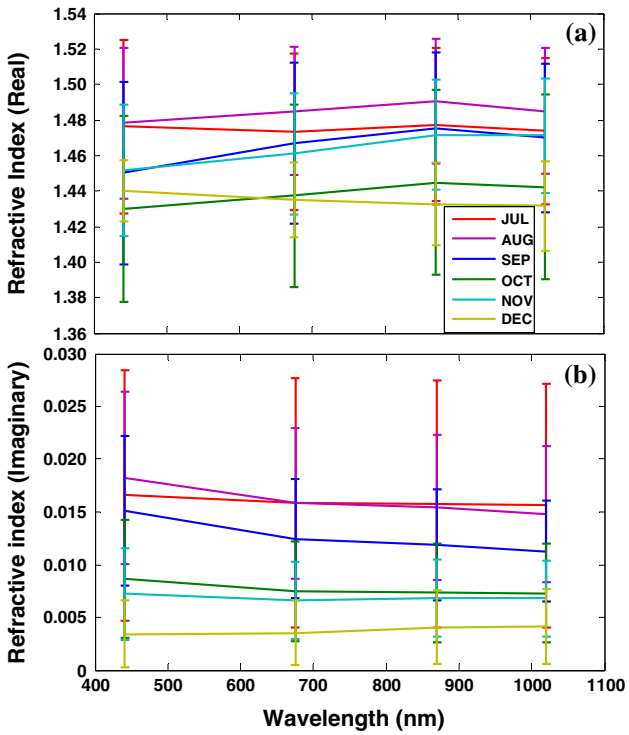

Fig. 7 Monthly mean variations of the real (**a**) and imaginary (**b**) parts of refractive indices as a function of wavelength

and October. The obtained values are comparable to the earlier published results reported by Dubovik et al. (2002) and Eck et al. (2003a) over Southern Africa.

3.5 Aerosol radiative forcing

The aerosol radiative forcing (ARF) at the top of the atmosphere (TOA) or at the surface/bottom (BOA) is defined as the difference in the net solar fluxes with and without aerosols. The difference between the BOA and TOA (BOA–TOA, in W m^{-2}) gives the radiative forcing in the complete atmosphere (ATM). In the present case, the net flux was computed in the wavelength ranging from 0.3 to 4.0 μm with and without aerosols at the TOA and at the BOA separately using the SBDART model (Ricchiazzi et al. 1998). The model SBDART is developed by Ricchiazzi et al. (1998) and is widely used by the atmospheric science community for the radiative transfer calculations (Alam et al. 2011, 2012; Sinha et al. 2013 and references therein). This model is dependent on DISORT module which is developed by Stamnes et al. (1988). In the present study, we run the model at 1-h interval for a 24-h period, and the integrated average forcing is estimated during clear sky days for every month during the period from July 2012 to December 2012 for Gorongosa. The parameters crucial for ARF estimations are AOD, SSA, ASY and surface albedo (Gadhavi and Jayaraman 2004). Other input

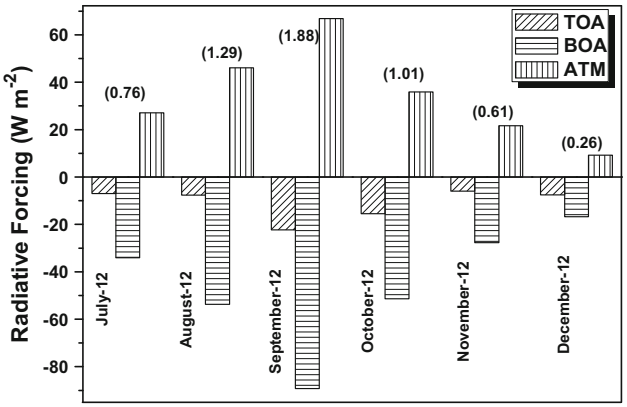

Fig. 8 Monthly averaged variations of simulated aerosol radiative forcing (W m^{-2}) at the TOA, BOA and within the atmosphere (ATM) at Gorongosa during the study period. Heating rates (K day^{-1}) are also shown in the figure within the parenthesis on the top of histograms for each month

parameters in the model include solar zenith angle, which is calculated using one small code in the SBDART (Ricchiazzi et al. 1998) by specifying a particular date, time, latitude and longitude, and atmospheric profiles (humidity, temperature, ozone and other gases). Based on the prevailing weather conditions and measured parameters, we used the mid-latitude summer atmospheric model. The AOD, SSA and ASY have been taken from the Gorongosa AERONET site and are used for the ARF calculations. The surface albedo values are obtained from the Aura OMI version 3 reflectivity data through the Giovanni online data system, developed and maintained by the NASA GES DISC (http://disc.gsfc.nasa.gov/giovanni).

The monthly average ARF variations computed from SBDART at TOA, BOA and ATM during the period of study are shown in Fig. 8. The monthly mean ARF at TOA, BOA and ATM is found to be in the range of −6 to −22 W m^{-2}, −16 to −89 W m^{-2} and +10 to +68 W m^{-2}, respectively. The averaged forcing for the entire period of observations at TOA is −11.01 W m^{-2}, while at the surface it is −45.46 W m^{-2}, leading to an atmospheric forcing of +34.45 W m^{-2}. In September 2012, the average forcing at the TOA and BOA, respectively, is −22 W m^{-2} and −89 W m^{-2}, giving rise to atmospheric forcing with an average value of +67 W m^{-2}. Likewise, the average ARF in August 2012 at BOA, TOA, and ATM is −54 W m^{-2}, −8 W m^{-2} and +46 W m^{-2}, respectively. In contrast to this, the average ARF is the minimum in the month of December 2012. The forcing at the BOA is −17 W m^{-2}, whereas, −7 W m^{-2} at the TOA and it is +9 W m^{-2} in the atmosphere.

The large differences in ARF between TOA and BOA demonstrate that solar radiation is absorbed within the atmosphere, consequently heating the atmosphere, reducing eddy heat convergence, and inducing a reduction in surface temperature (Ge et al. 2010). Furthermore, heating due to absorption of solar radiation by aerosols reaches its maximum close to its uppermost level where the heating is stabilised, which in turn may suppress convective activity and prevent cloud formation (Ackerman et al. 2000; Koren et al. 2004). The ARF values are the highest for the month of September 2012 due to the frequent biomass burning activities and local anthropogenic activities. It can be concluded that the presence of BC aerosols over Mozambique can considerably decrease at the BOA and TOA forcing and enhance the atmospheric forcing. Alam et al. (2011) reported over Karachi that the ARF at the TOA, BOA and ATM is in the range of −7 to −35 W m^{-2}, −56 to −96 W m^{-2} and +38 to +61 W m^{-2}, respectively. Ge et al. (2010) found the surface forcing ranging from −7.9 to −35.8 W m^{-2} over Northwestern China. Kim et al. (2005) also estimated the ARF which lies between −13 and −43 W m^{-2} for three ground sites in Eastern Asia, which is lower than the results obtained in the present study.

The atmospheric heating rate can be estimated by following Liou (2002) as

$$\frac{\partial T}{\partial t} = \frac{g}{C_P}\frac{\Delta F_{ATM}}{\Delta P} \quad (2)$$

where ∂T/∂t is the heating rate (°K day^{-1}), g is the acceleration due to gravity, ΔF_{ATM} is the atmospheric heating, C_p is the specific heat capacity of air at constant pressure and ΔP is the atmospheric pressure. The average heating rate (°K day^{-1}) over Gorongosa during the winter and spring, respectively, is 1.03 and 1.17 (see Fig. 8). The maximum heating rate noticed in the month of September (1.88 K day^{-1}) was attributed to high atmospheric absorption due to increase in the concentration of BC aerosols generated from biomass burning activity.

Table 2 shows comparisons of ARFs obtained at the BOA and TOA from AERONET to SBDART calculations. The forcing at the TOA is higher in magnitude for AERONET as compared to SBDART during the study period and comparable for the month of December. Likewise, the forcing at the BOA is higher (more negative) in September for SBDART than the AERONET, whereas for other months the forcing at BOA for AERONET and SBDART is almost nearly comparable. The correlation coefficient (R^2) for the whole period of observation for AERONET vs. SBDART at the BOA and TOA is 0.95 and 0.97, respectively. Overall, the comparison shows a convincing agreement for the radiative forcing at the BOA and TOA obtained from AERONET to SBDART. A significant difference has been revealed between the two values as this is due to assumption of inputs in the SBDART model.

Table 2 Comparison of ARFs of AERONET and SBDART at the BOA and TOA over Gorongosa during the study period

Month	SBDART calculated ARF		AERONET derived ARF	
	TOA ($W\ m^{-2}$)	BOA ($W\ m^{-2}$)	TOA ($W\ m^{-2}$)	BOA ($W\ m^{-2}$)
July	−6.99	−34.05	−11.02	−41.36
August	−7.67	−53.73	−14.83	−58.98
September	−22.36	−89.22	−20.33	−80.11
October	−15.46	−51.37	−22.16	−66.03
November	−6.01	−27.66	−13.16	−33.59
December	−7.53	−16.71	−9.36	−21.43

4 Conclusions

The monthly variability in the aerosol optical and microphysical properties over Gorongosa is very significant to understand the impact of fine aerosols produced from biomass burning on regional atmosphere and climatic forcing, although the data size (6 months) is not sufficient to establish definite aerosol climatology of the region. The major findings in the present study can be summarised as follows:

The monthly mean AOD_{500} ranges between 0.20 ± 0.06 and 0.64 ± 0.34, attaining peak in September and the CWV ranges between 1.88 ± 0.28 and 4.02 ± 0.77 increasing constantly during the study period. The Ångström exponent increased from July with its maximum of 1.56 ± 0.26 in the month of September implying the dominance of fine-mode aerosol and started to decrease from October (1.48 ± 0.44) onwards through December (0.76 ± 0.34) showing an increasing dominance of coarse-mode aerosol (relatively smaller amount of fine aerosol). The AODs obtained from AERONET are compared with MODIS-retrieved AODs computed for the same wavelength and the correlation coefficient R^2 was found to be 0.80 and 0.89 for Terra and Aqua-MODIS, respectively, during the study period.

The volume size distribution (VSD) of aerosols showed a bimodal lognormal structure with fine aerosol having the radius between 0.1 and 0.2 μm and the coarse mode from 2.0 to 6.0 μm. The fine mode remains higher from August to October, while the coarse mode is higher in December. The SSA ranges between 0.87 and 0.94 in the wavelength region (440–670 nm) and decreased in wavelength from July to October because of the relative abundance of fine aerosol (absorbing in nature) generated from biomass burning events. The asymmetry parameter decreases with wavelength in the visible region from July to October and increases in near-IR during November and December indicating a shift in dominance from fine-mode to coarse-mode aerosols. The real and imaginary refractive indices indicated the presence of mixed type of aerosols over the study region. The optical state of the atmosphere over the measurement region dominated with absorbing aerosol for the study period especially in the months from July to September, as the imaginary refractive index lies above 0.01.

The present investigation also carried out to study the effect of aerosols on shortwave radiative forcing over Gorongosa using SBDART model. The average forcing for the entire study period was found to be $-11.01\ W\ m^{-2}$ at TOA, $-45.46\ W\ m^{-2}$ at BOA and ARF of $+34.45\ W\ m^{-2}$ with an average heating rate of $0.97\ K\ day^{-1}$ for period July–December, 2012. Finally, the comparison shows good agreement between the ARFs at the BOA and TOA obtained from AERONET to SBDART.

Acknowledgments The authors sincerely thank UKZN, South Africa and NUIST, China for providing enabling environment and infrastructure support to carry out the present work. This work was partly supported by the National Research Foundation (NRF–South Africa) bi-lateral research grant (UID: 78682). Authors are indebted to the AERONET team of NASA, USA for their efforts in making the data available online. We gratefully acknowledge Prof. Brent N. Holben, PI and Dr. Marc Stalmans, site manager of Gorongosa site and their staff effort in establishing and maintaining AERONET site related to this investigation. One of the authors KRK expresses profound gratitude to Yan Yin, Diao Yiwei, Na Kang, Xingna Yu and Liang Xuewei for their support and cooperation. The authors would like to thank the editor and the two anonymous reviewers for their insightful comments and constructive suggestions which in turn helped to improve the clarity and scientific content of the original paper.

References

Ackerman AS, Toon OB, Stevens DE, Heymsfield AJ, Ramanathan V, Welton EJ (2000) Reduction of tropical cloudiness by soot. Science 288:1042–1047

Adesina AJ, Kumar KR, Sivakumar V, Griffith D (2014, In Press) Direct radiative forcing of urban aerosols over Pretoria (25.75°S, 28.28°E) using AERONET Sunphotometer data: first scientific results and environmental impact. J Environ Sci (in press)

Alam K, Trautmann T, Blaschke T (2011) Aerosol optical properties and radiative forcing over mega-city Karachi. Atmos Res 101: 773–782

Alam K, Trautmann T, Blaschke T, Majid H (2012) Aerosol optical and radiative properties during summer and winter season over Lahore and Karachi. Atmos Environ 50:234–245

Andrews R, Sheridan P, Fiebig M, McComiskey A, Ogren J, Arnott P et al (2006) Comparison of methods for deriving aerosol asymmetry parameter. J Geophys Res 111(D5). doi:10.1029/2004JD005734

Ångström A (1961) Techniques of determining the turbidity of the atmosphere. Tellus 13:214–223

Archibald S, Staver AC, Levin SA (2012) Evolution of human driven fire regimes in Africa. Proc Natl Aca Sci 109(3):847–852

Arola A, Lindfors A, Natunen A, Lehtinen KEJ (2007) A case study on biomass burning aerosols: effects on aerosol optical and surface radiation levels. Atmos Chem Phys 7:4257–4266

Arola A, Schuster G, Myhre G, Kazadzis S, Dey S, Tripathi S (2011) Inferring absorbing organic carbon content from AERONET data. Atmos Chem Phys 11(1):215–225

Babu SS, Moorthy KK, Manchanda RK, Sinha PR, Satheesh SK, Prasad VD, Srinivasan S, Arunkumar VH (2011) Free tropospheric black carbon aerosol measurements using high altitude balloon: Do BC layers build 'their own homes' up in the atmosphere? Geophys Res Lett 38(L08803). doi:10.1029/2011GL046654

Badarinath KVS, Latha KM, Chand TRK, Gupta PK (2009) Impact of biomass burning on aerosol properties over tropical wet evergreen forests of Arunachal Pradesh, India. Atmos Res 91:87–93

Bi J, Huang J, Fu Q, Wang X, Shi J, Zhang W et al (2011) Toward characterization of the aerosol optical properties over Loess Plateau of Northwestern China. J Quant Spec Rad Trans 112(2):346–360

Bond TC, Doherty SJ, Fahey DW, Forster PM, Berntsen T, De Angelo BJ, Flanner MG, Ghan S, et al. (2013) Bounding the role of black carbon in the climate system: a scientific assessment. J Geophys Res 118. doi:10.1002/jgrd.50171

Charlson RJ, Schwartz SE, Hales JH, Cess RD, Coakley JA Jr, Hansen JE, Hofmann DJ (1992) Climate forcing by anthropogenic aerosols. Science 255:423–430

D'Almeida GA, Koepke P, Shettle EP (1991) Atmospheric aerosols: Global climatology and radiative characteristics (studies in geophysical optics and remote sensing). A Deepak Publishing, Hampton

Draxler RR, Rolph GD (2003) HYSPLIT (HYbrid Single-Particle Lagrangian Integrated Trajectory) Model access via NOAA ARL READY Website (http://www.arl.noaa.gov/ready/hysplit4.html) NOAA Air Resources Laboratory, Silver Spring, MD, USA

Dubovik O, King MD (2000) A flexible inversion algorithm for retrieval of aerosol optical properties from sun and sky radiance measurements. J Geophys Res 105:20673–20696

Dubovik O, Smirnov A, Holben BN, King MD, Kaufman YJ, Eck TF, Slutsker I (2000) Accuracy assessments of aerosol optical properties retrieved from aerosol robotic network (AERONET) sun and sky radiance measurements. J Geophys Res 105:9791–9806

Dubovik O, Holben BN, Eck TF, Smirnov A, Kaufman YJ, King MD et al (2002) Variability of absorption and optical properties of key aerosol types observed in worldwide locations. J Atmos Sci 59(3):590–608

Eck TF, Holben BN, Reid JS, Dubovik O, Smirnov A, O'Neill NT et al (1999) Wavelength dependence of the optical depth of biomass burning urban and desert dust aerosols. J Geophys Res 104:31333–31350. doi:10.1029/1999JD900923

Eck TF, Holben BN, Ward D, Mukelabai M, Dubovik O, Smirnov A et al (2003a) Variability of biomass burning aerosol optical characteristics in southern Africa during the SAFARI 2000 dry season campaign and a comparison of single scattering albedo estimates from radiometric measurements. J Geophys Res 108(D13). doi:10.1029/2002JD002321

Eck TF, Holben BN, Reid J, O'Neill N, Schafer J, Dubovik O et al (2003b) High aerosol optical depth biomass burning events: a comparison of optical properties for different source regions. Geophys Res Lett 30(20). doi:10.1029/2003GL017861

Eck TF, Holben BN, Reid JS, Mukelabai MM, Piketh SJ, Torres O, Jethva HT et al (2013) A seasonal trend of single scattering albedo in southern African biomass-burning particles: implications for satellite products and estimates of emissions for the World's largest biomass-burning source. J Geophys Res 118:6414–6432. doi:10.1002/jgrd.50500

Gadhavi H, Jayaraman A (2004) Aerosol characteristics and aerosol radiative forcing over Maitri, Antarctica. Curr Sci 86:296–304

Gadhavi H, Jayaraman A (2010) Absorbing aerosols: contribution of biomass burning and implications for radiative forcing. Anna Geophys 28:103–111

Ge JM, Su J, Ackerman TP, Fu Q, Huang JP, Shi JS (2010) Dust aerosol optical properties retrieval and radiative forcing over northwestern China during the 2008 China–US joint field experiment. J Geophys Res 115(D00k12). doi:10.1029/2009JD013263

Gupta P, Gadhavi H, Jayaraman A (2003) Aerosol optical depth variation observed using sun-photometer over Indore. Ind J Rad Spac Phys 32:229–237

Hess M, Koepke P, Schult I (1998) Optical properties of aerosols and clouds: the software package OPAC. Bull Amer Meteo Soc 79:831–844

Holben BN, Eck TF, Slutsker I, Tanre D, Buis J et al (1998) AERONET: a federated instrument network and data archive for aerosol characterization. Rem Sens Environ 66(1):1–16

Holben BN, Eck TF, Slutsker I, Smirnov A, Sinyuk A, Schafer JS, et al. (2006) Aeronet's Version 2.0 quality assurance criteria. Proc SPIE 6408(64080Q). doi:10.1117/12.70652

Jayaraman A, Lubin D, Ramachandran S, Ramanathan V, Woodbridge E, Collins WD, Zalpuri KS (1998) Direct observations of aerosol radiative forcing over the tropical Indian Ocean during the January–February 1996 pre-INDOEX cruise. J Geophys Res 103:13827–13836

Jayaraman A, Gadhavi H, Ganguly D, Misra A, Ramachandran S, Rajesh TA (2006) Spatial variations in aerosol characteristics and regional radiative forcing over India: measurements and modelling of 2004 road campaign experiment. Atmos Environ 40:6504–6515

Kalnay E, Kanamitsu M, Kistler R, Collins W et al (1996) The NCEP/NCAR reanalysis 40-year project. Bull Amer Meteo Soc 77:437–471

Kim DOH, Sohn BJ, Nakajima T, Takamura T (2005) Aerosol radiative forcing over east Asia determined from ground-based solar radiation measurements. J Geophys Res 110(D10S22). doi:10.1029/2004JD004678

Koren I, Kaufman YJ, Remer LA, Martins JV (2004) Measurement of the effect of Amazon smoke on inhibition of cloud formation. Science 303:1342–1345

Kumar KR, Narasimhulu K, Balakrishnaiah G, Reddy LSS, Gopal KR, Reddy RR, Satheesh SK, Moorthy KK, Babu SS (2010) A study on the variations of optical and physical properties of aerosols over a tropical semi-arid station during grassland fire. Atmos Res 95:77–87

Kumar KR, Sivakumar V, Reddy RR, Gopal KR, Adesina AJ (2013) Inferring wavelength dependence of AOD and Ångström exponent over a sub-tropical station in South Africa using AERONET data: influence of meteorology, long-range transport and curvature effect. Sci Tot Environ 461–462:397–408

Liou KN (2002) An Introduction to atmospheric radiation. Elsevier, New York, p 583

Ogunjobi K, He Z, Simmer C (2008) Spectral aerosol optical properties from AERONET Sunphotometric measurements over West Africa. Atmos Res 88(2):89–107

Penner JE, Dickinson RE, O'Neill CA (1992) Effects of aerosol from biomass burning on the global radiation budget. Science 256:1432–1434

Queface AJ, Piketh SJ, Eck TF, Tsay SC, Mavume AF (2011) Climatology of aerosol optical properties in Southern Africa. Atmos Environ 45:2910–2921

Ramachandran S, Rajesh TA (2008) Asymmetry parameters in the lower troposphere derived from aircraft measurements of aerosol scattering coefficients over tropical India. J Geophys Res 113(D16). doi:10.1029/2008JD009795

Ramanathan V, Crutzen PJ, Kiehl JT, Rosenfeld D (2001) Aerosol, climate, and the hydrological cycle. Science 294:2119–2124

Ranjan RR, Joshi HP, Iyer KN (2007) Spectral variation of total column aerosol optical depth over Rajkot: a tropical semi-arid Indian station. Aero Air Qual Res 7:33–45

Ricchiazzi P, Yang S, Gautier C, Sowle D (1998) SBDART: a research and teaching software tool for plane-parallel radiative transfer in the earth's atmosphere. Bull Amer Met Soc 79:2101–2114

Roberts JM, Veres PR, Cochran AK, Warneke C, Burling IR, Yokelson RJ et al (2011) Isocyanic acid in the atmosphere and its possible link to smoke related health effects. Proc Natl Aca Sci 108(22):8966–8971

Rosenfeld D, Rudich Y, Lahav R (2001) Desert dust suppressing precipitation: a possible desertification feedback loop. Proc Natl Acad Sci USA 98:5975–5980

Satheesh SK, Moorthy KK (2005) Radiative effects of natural aerosols: a review. Atmos Environ 39:2089–2110

Shaw GE (1983) Sun photometry. Bull Amer Meteo Soc 64:4–10

Simrnov A, Holben BN, Dubovik O, O'Neill NT, Eck TF, Westphal DL et al (2002) Atmospheric aerosol optical properties in the Persian Gulf. J Atmos Sci 59(3):620–634

Sinha PR, Dumka UC, Manchanda RK, Kaskaoutis DG, Sreenivasan S, Moorthy KK, Babu SS (2013) Contrasting aerosol characteristics and radiative forcing over Hyderabad, India due to seasonal mesoscale and synoptic-scale processes. Quar J Roy Meteo Soc 139:434–450

Sivakumar V, Tesfaye M, Alemu W, Sharma A, Bollig C, Mengistu G (2010) Aerosol measurements over South Africa using satellite, sun-photometer and LIDAR. Adv Geosci 16:253–262

Srivastava A, Tiwari S, Devara PCS, Bisht D, Srivatsava MK, Tripathi S et al (2011) Pre-monsoon aerosol characteristics over the Indo-Gangetic Basin: implications to climatic impact. Ann Geophys 29:789–804

Stamnes K, Tsay S, Wiscombe W, Jayaweera K (1988) Numerically stable algorithm for discrete-ordinate-method radiative transfer in multiple scattering and emitting layered media. Appl Opt 27:2502–2509

Suman MNS, Gadhavi H, Kiran VR, Jayaraman A, Rao SVB (2013) Role of coarse and fine mode aerosols in MODIS AOD retrieval: a case study. Atmos Meas Tech Diss 6:9109–9132

Sumit Kumar, Devara PCS, Sonbawne S, Saha S (2011) Sun-sky radiometer derived column integrated aerosol optical and physical properties over a tropical urban station during 2004–2009. J Geophys Res 116(D10201). doi:10.1029/2010JD014944

Tesfaye M, Sivakumar V, Botai J, Tsidu GM (2011) Aerosol climatology over South Africa based on 10 years of Multiangle Imaging Spectroradiometer (MISR) data. J Geophys Res 116(D20216). doi:10.1029/2011JD16023